Geological Magazine

www.cambridge.org/geo

Microphytoplankton biometry as prospective vector for sulphide ore deposits: a case study in the Iberian Pyrite Belt

Felipe González, Reinaldo Sáez and Carmen Moreno

Earth Science Department, University of Huelva, Huelva, Spain

Original Article

Cite this article: González F, Sáez R, and Moreno C. Microphytoplankton biometry as prospective vector for sulphide ore deposits: a case study in the Iberian Pyrite Belt. *Geological Magazine* **162**(e17): 1–12. https://doi.org/10.1017/S0016756825100034

Received: 9 December 2024
Revised: 27 April 2025
Accepted: 6 May 2025

Keywords:
Iberian Pyrite Belt; Late Devonian; black shales; phytoplankton; biometry; mineral exploration

Corresponding author:
Felipe González; Email: fbarrio@uhu.es

Abstract

The Iberian Pyrite Belt contains one of the largest accumulations of massive sulphide deposits on Earth. Many of these deposits are hosted by latest Devonian black shales rich in terrestrial and marine palynomorphs. Among the marine fossils, the most abundantly reported species is *Maranhites mosesii*. By means of a multi-analytical methodology, including (1) biometry of specimens, (2) TOFSIMS imaging and spectral analysis of selected specimens and (3) host-rock geochemistry, we detected that cysts of *M. mosesii* are smaller and lighter in massive sulphide-generating environments than in coeval non-massive sulphide-generating environment. Cysts of *M. mosesii* sank after encystment and maturated in the seafloor of different subbasins affected by disparate anoxic conditions. The specimens that maturated in anoxic settings enriched in pollutants, like Arsenic (As) and Lead (Pb), were smaller and lighter than those from non-polluted anoxic environments. Their organic walls were also enriched in As. Neither the anoxia nor the pollutants prevented the proliferation of *M. mosesii*, as this was the most abundant phytoplanktonic species in all environments. To explain this, we suggest that this species developed a successful adaptive mechanism that might involve anaerobic metabolic interchange with the surrounding oxygen-depleted media and high levels of tolerance to stressors. Whatever the reason, it entails a causal relationship between cyst size and seafloor environmental conditions. In consequence, the biometry of *M. mosesii* can be envisaged as a promising vector for sulphide deposit exploration in the Iberian Pyrite Belt.

1. Introduction

The Iberian Pyrite Belt (IPB), located at the southwest margin of the Iberian Peninsula, contains one of the largest accumulations of massive sulphide deposits in the world. The original reserves of this Devonian-Carboniferous basin have been estimated at 1700 Mt of massive sulphides and 300 Mt of stockwork-type mineralization. Ores are primarily composed of pyrite with minor amounts of base metal sulphides (chalcopyrite, sphalerite and galena), other sulphides (including arsenopyrite) and sulfosalts. Besides Cu, Zn and Pb, important reserves of Sn, Au and Ag have been also documented. Mining exploitation in the region dates back over 5000 years. During this time, 82 sulphide deposits have been mined and several other indications have been documented (Pinedo Vara 1963; Sáez *et al.* 1996; 1997; 2024; Leistel *et al.* 1998; Tornos *et al.* 2000; Almodóvar *et al.* 2019; Sáez *et al.*, 2024).

At the latest Devonian, the environmental conditions of the hitherto stable IPB were drastically conditioned by the basin breakup and compartmentation associated with the onset of the Variscan cycle in the region (Moreno *et al.*, 1996; Soriano & Casas, 2002; Oliveira *et al.* 2004, 2019). The resulting IPB configuration consisted of a puzzling framework of coeval sub-basins filled with black shales, variable amounts of volcanic rocks and, on many occasions, large accumulations of massive sulphides (Moreno *et al.* 1996; Leistel *et al.* 1998; Sáez *et al.* 1999). These sub-basins, currently obscured by tectonic overprint, achieved disparate environmental conditions, and their black shales generally contain abundant spores and organic-walled microphytoplankton (González *et al.* 2005*a*; 2005*b*; Sáez *et al.* 2008; Pereira *et al.* 2021; 2023; Mendes *et al.* 2024). Among the marine organisms, the most prominently reported species is *Maranhites mosesii* (Sommer) Brito 1967 emend Gonzalez 2009.

Other microphytoplankton species found in the IPB, including acritarchs and prasinophyte microalgae, can be locally abundant, but for yet unknown reasons *M. mosesii* is by far the most widely and abundantly reported species in the region (González *et al.* 2005; González, 2009; Mendes *et al.* 2024).

According to González (2009), this microphytoplankton species exhibits high morphological variability linked to its ontogenetic development. However, while intra-sample size variations may be attributed to this growth trend, *M. mosesii* specimens from the IPB show significant inter-sample size disparities that are difficult to explain exclusively by this phenomenon. The present study provides the biometric analysis of populations of *M. mosesii* obtained from

different localities, specifically from coeval massive sulphide-generating environments (MSGE) and non-massive sulphide-generating environments (non-MSGE). Geochemical analysis of the hosting black shales and Time-of-Flight Secondary Ion Mass Spectrometry (ToF-SIMS) spectra of a selection of specimens representative of each environment provide insights into the origin of this morphological disparity. The casual/causal relationship between morphological variation and presence/absence of massive sulphides in the hosting environments is thus explored.

To date, the information provided by the palynological analysis of the black shales hosting the IPB massive sulphides has been instrumental in biostratigraphically constraining the oldest mineralization event. Miospore assemblages invariably attributed to the uppermost Devonian Biozone of Western Europe, *Retispora lepidophyta-Verucosisporites nitidus* (LN) by Streel *et al.* (1987), have been reported in the shales hosting the massive sulphides of Aznalcóllar (Pereira *et al.* 1996), Neves-Corvo (Pereira & Pacheco, 2004, 2021; Mendes *et al.* 2024), Tharsis (González *et al.* 2002), Sotiel Coronada (González *et al.* González *et al.*, 2006), Torerera, Las Herrerías (Sáez *et al.,* 2008), Caveira (Matos *et al.* 2014), Semblana-Rosa Magra and Monte Branco (Pereira *et al.* 2021). The multi-analytical approach here proposed represents a step forward, as it examines the viability of considering the morphology of *M. mosesii* as a prospecting method to discriminate between mineralized and barren sequences within the IPB.

2. Geological setting

The IPB is the largest and most representative domain comprising the South Portuguese Zone in the southern margin of the Iberian Variscan Massif (Figure 1a). Its stratigraphic record extends from Middle Devonian to Late Mississippian (González *et al.* 2003; Mendes *et al.* 2020; 2024; Moreno & González, 2004; Pereira *et al.* 2021) comprising three lithostratigraphic units (Schermerhörn, 1971). From footwall to hanging wall, these are: Phyllite-Quartzite Group (PQ Group), Volcanic-Sedimentary Complex (VSC) and Culm Group (referred to in Portugal as Baixo Alentejo Flysch Group) (Figures 1a and 2). The PQ Group consists of a thick detrital sequence of shales and sandstones, Givetian–latemost Famennian in age, deposited in a stable and shallow siliciclastic platform, eventually affected by storms (Sáez & Moreno, 1997; Matos *et al.* 2014; Oliveira *et al.* 2013; 2019). To the top, the series incorporates isolated limestone bodies (see, for example, van den Boogaard, 1963; van den Boogaard & Schermerhörn, 1981; Albardeiro *et al.* 2020; Mendes *et al.* 2020) and conglomerates, as well as mega debris-flow and fan-delta deposits, all in relation with the instability affecting the IPB during early propagation of the Variscan cycle (Moreno *et al.* 1996). Such instability resulted in the Late Devonian fragmentation and compartmentation of the IPB basin. The transition between the PQ Group and the VSC is commonly associated with a black shale sequence rich in organic matter including minor interbedded volcanics. This so-called anoxic sequence (Moreno & González, 2004) hosts many of the large massive sulphide deposits from the southern part of the region, including Tharsis, Sotiel Coronada-Migollas, Aznalcóllar-Los Frailes, Neves-Corvo, Lousal and Carveira. Above the anoxic sequence, the VSC incorporates a diversity of Mississippian sedimentary volcanic and subvolcanic rocks, mafic and felsic in nature, displaying frequent thickness variations and abrupt lateral and vertical facies changes. This unit is interpreted in relation to the transtensional effect of the early syn-orogenic stage occurring in a heterogeneous and compartmentalized basin (Moreno *et al.* 1996; Martín-Izard *et al.* 2017; Oliveira *et al.* 2019).

Sulphide deposits from the north and intermediate zones of the IPB are mostly associated with volcanic and volcaniclastic rocks of the VSC. The geochronological constrain of these deposits is still poor, but limited available data indicate a late Tournaisian age (Barrie *et al.* 2002; Dunning *et al.* 2002; Albardeiro *et al.* 2023). Considering all the biostratigraphic and geochronological age data, the existence of two mineralizing pulses (late Famennian and late Tournaisian) or a single continuous metallogenic episode extending from late Famennian to late Tournaisian is still under debate (Albardeiro *et al.* 2020; 2023; Sáez *et al.* 2024).

The contact between the VSC and the overlying Culm Group is marked by another shaly sequence, the Basal Shaly Formation (Moreno & Sequeiros, 1989), referred to in Portugal as the Brancanes Formation (Oliveira *et al.* 2013, 2019). This unit comprises reworked material from the uppermost VSC intervals, along with siliciclastic deposits linked to the initial post-volcanic turbiditic pulses in the region. Above this formation, the Culm Group comprises the syn-orogenic infill of the IPB basin (Moreno, 1993; Moreno *et al.* 1996; Oliveira, 1990; 2019). During the Asturian phase of the Variscan orogeny, the entire succession was deformed following a thin-skinned tectonic style (Silva *et al.* 1990).

The four sampling sites selected in this study are stratigraphically located within the anoxic sequence transitional between the PQ Group and VSC (Figure 2). All samples collected in these sites were palynostratigraphically analyzed and attributed to the uppermost Famennian LN Miospore Biozone (Streel *et al.* 1987) of Western Europe. Two of the studied sites, Tharsis and Sotiel, are located in MSGE, whereas the other two, Águila Range and Calañas, are from non-MSGE (Figure 1). Samples from non-MSGE are outcrop samples. Those from Tharsis and Sotiel are, respectively, from an open pit and from an underground mine. The stratigraphic location of the samples studied in each locality is illustrated in Figure 1b. Details of the biostratigraphic analysis carried out on each site can be seen in González *et al.* (2002, 2005, González *et al.*, 2006) and Moreno *et al.* (2003).

3. Materials and methods

The analysis performed on all the samples includes biometry, Time-of-Flight Secondary Ion Mass Spectrometry (TOF-SIMS) of selected *M. mosesii* specimens and geochemical analysis of the hosting black shales. Biometry and TOF-SIMS were preceded by a palynological extraction procedure, which essentially followed the standard tri-acid digestion method described by Wood *et al.* (1996). This comprises initial disaggregation of approx. 35 g of sample, immersion in HCl (36%) to remove carbonates, dissolution of silicate minerals with hot HF (40%) and a second immersion into hot HCl (36%) to eliminate fluorides and remaining carbonates. After neutralization, the organic residue was oxidized with Schulze solution for variable time intervals. The oxidized residue was mounted in microscope slides using Cellosize as dispersant and Elvacite as mounting medium. Preservation status of the selected samples was optimal for palynological identification. After biostratigraphic recognition and palynofacies analysis, based on 350 counts, the biometry of *M. mosesii* was performed selecting 120 specimens per sample, when possible. The morphological features measured were: vesicle diameter, equatorial pads, equatorial embayment, lateral thickenings and translucent bladders. Details on these structural elements can be seen in Figure 3 and in González (2009). Biostratigraphy, palynofacies and

https://doi.org/10.1017/S0016756825100034 Published online by Cambridge University Press

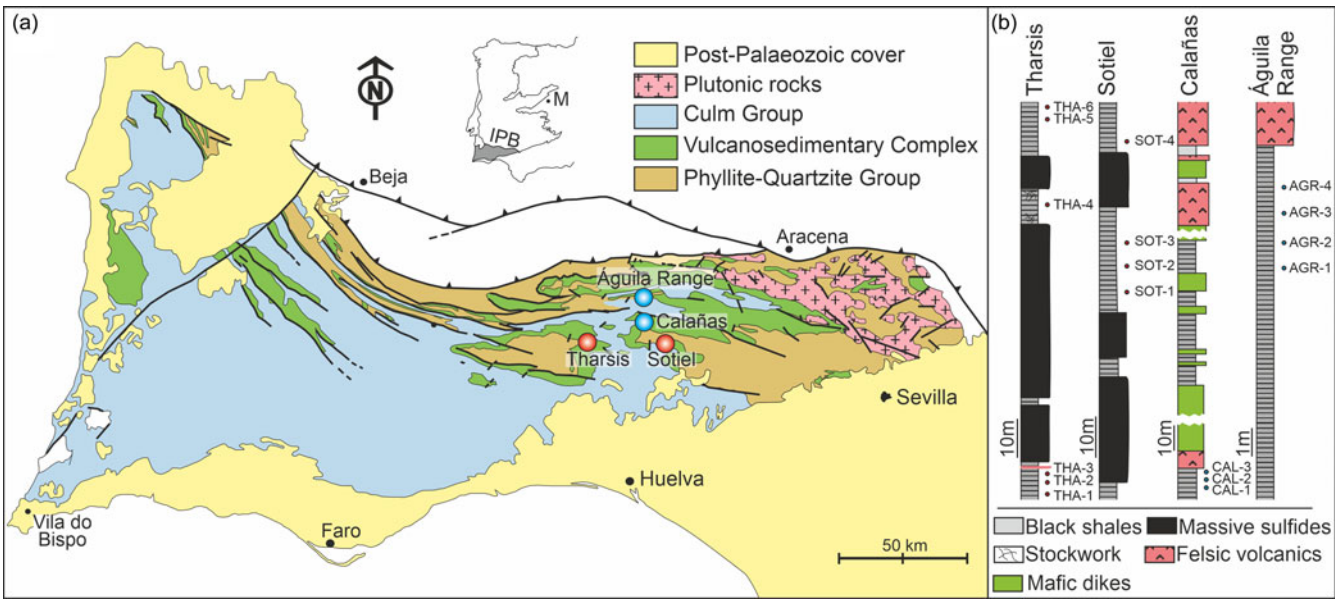

Figure 1. (a) Geological sketch map of the Iberian Pyrite Belt (IPB) with indication of the four sub-environments/sub-basins considered in this study. M, Madrid; IPB, Iberian Pyrite Belt. Red circles indicate MSGE. Blue circles indicate non-MSGE. (b) Stratigraphic logs at these localities showing the location of the studied samples. All the samples are latest Famennian (LN Biozone) in age.

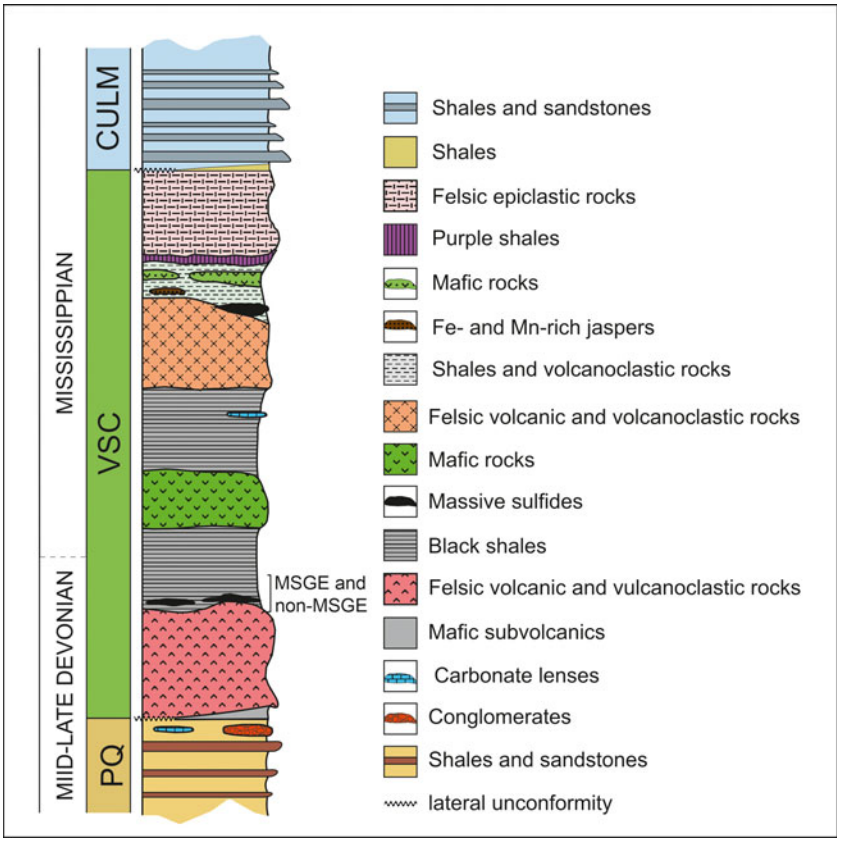

Figure 2. Synthetic stratigraphic log of the IPB.

biometric analyses were performed in the Department of Earth Sciences, University of Huelva, using a Nikon Labaphot-2 microscope equipped with the digital camera Nikon DS-Fi1 (Software NIS Elements, F Package, 3.22.00). Processed and remaining unprocessed samples are deposited in the collections of the Earth Sciences Department, University of Huelva.

For the TOF-SIMS analysis, 20–40 specimens per sample of *M. mosesii* were picked with a micromanipulator needle and

https://doi.org/10.1017/S0016756825100034 Published online by Cambridge University Press

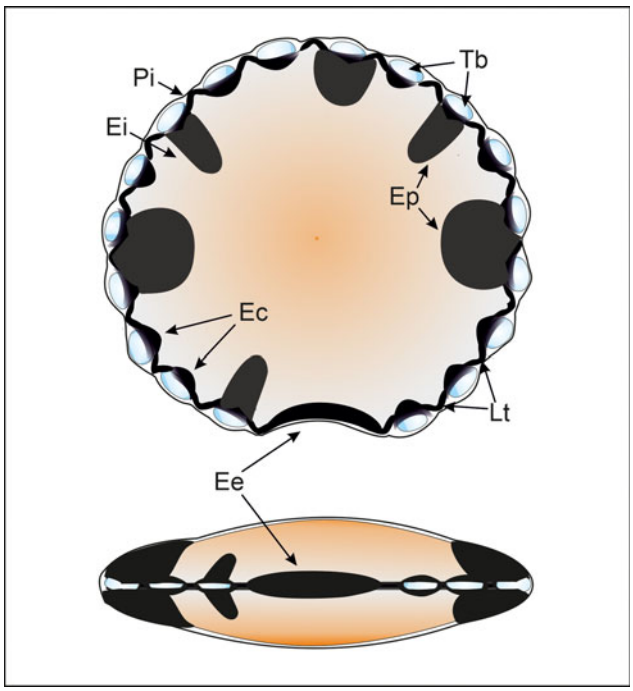

Figure 3. Polar and equatorial scheme views of *M. mosesii* after González (2009) with indication of its main equatorial structures: (Pi) Perieilyma. Outer vesicle wall; (Ei) Endeilyma. Inner vesicle wall; (Ep) Equatorial pads. Solid, protrusive discrete to rarely interconnected structures, circular to subcircular in outline; (Ec) Embracing cells. Dark equatorial structures, elliptical to subircular in outline, that enclose translucent bladders and are connected by lateral thickening; (Lt) Lateral thickening. Small, solid, circular, subcircular or arcuate structures that connect embracing cells; (Tb) Translucent bladders. Hollow, rounded to elliptical equatorial structures, enclosed by embracing cells, that progressively enlarge during vesicle maturation; (Ee) Equatorial embayment, normally thickened, that may or may not be accompanied by embracing cells or equatorial pads.

mounted in a double-sided Cu tape. Measurement and chemical imagery were then performed using a TOF-SIMS IV instrument (ION-TOF GmbH, Germany) located at the Scientific and Technological Research Assistance Centre of the University of Vigo, Spain. The analysis was carried out with a primary ion beam of 25 KeV Bi^{3+} (pulsed current between 0.12 and 0.15 pA) scanning over a 500 × 500 μm^2 area for 100–150 s. The Primary Ion Dose Density was settled to be below the static limit (1013 ions/cm^2). A pulsed electron flood gun source was employed for surface build up charge compensation.

Spectra (m/z 0–1000) and chemical maps of selected m/z values (scans acquisition repeated 75 times) were collected for all samples in positive and negative polarity. Positive and negative ion spectra were internally mass-calibrated using CH_3^+, $C_2H_3^+$, $C_3H_5^+$ and $C_5H_{14}NO$ peaks for positive ions, and CH^-, C_2H^-, C_4H^- and $C_{18}H_{35}O_2^-$ peaks for negative ions, respectively. Deviation between theoretical and measured masses was always below 100 ppm. Combining the elements described in the literature as potential contaminant for phytoplankton with those that could be mobilized in oxygen-depleted and/or hydrothermally influenced environments, the list of major and trace elements searched in TOF-SIMS profiles includes Mg, Al, Si, Cr, Fe, Co, Zn, As, Cd, Cs, Ba, Ce, Cu, Hg and Pb.

Chemical composition of shales was obtained after milling on agate mortar and split into 20 g fractions at the University of Huelva laboratories. Geochemistry was characterized by analyzing major and trace elements together with carbon and sulphur in a fully certified commercial laboratory (ACME, Analytical Laboratories, Vancouver, Canada). Total abundances of major oxides were determined by ICP emission spectrometry. Rare Earth and refractory elements were analyzed by ICP mass spectrometry. Both procedures followed Li-metaborate/tetraborate fusion and dilute nitric digestion of samples weighing 0.2 g. Sample splits of 0.5 g were analyzed for a selection of metals and semi-metals including Cu, Pb, Zn, As, Se and Hg after aqua regia digestion. Sulphur, total C and organic C were determined by Leco analysis.

4. Results

4.a. Maranhites mosesii

The microphytoplankton species *M. mosesii* extends from Early Devonian to Mississippian. It is widely distributed throughout Gondwana and southern margin of Laurussia and is generally associated with shallow marine depositional environments, relatively close to emergent landmasses (González, 2009). Morphologically, it consists of a vesicle, originally discoidal, circular to subcircular in outline, 40 to 200 µm in diameter and two-layered. The inner layer (endeilyma), noticeably thicker than the outer layer (perieilyma), contains well-differentiated structural elements at equatorial positions, including solid pads, embracing cells, transparent bladders, lateral thickenings and an equatorial embayment (Figure 3).

The ontogenetic trend detected in *M. mosesii* (González, 2009) entails increasing vesicle size and continuous transformation of these equatorial structures. Growth trends also involving vesicle enlargement have been described in cyst-forming prasinophyte species during their non-motile stage (Tappan, 1980; Knoll *et al.* 1991; Teyssèdre, 2006; Taylor *et al.* 2009). As in prasinophytes, the progressive cyst enlargement of *M. mosesii* cannot be solely attributed to the consumption of internal reserves, necessitating metabolic exchange with the surrounding environment.

The biometric analysis of *M. mosesii* shows that the average equatorial diameter and the number of pads-bearing specimens clearly differ between MSGE and non-MSGE (Figure 4). In samples from the two MSGE selected in this study (Figures 1 and 2), the average equatorial diameter of *M. mosesii* specimens ranges from 68.2 to 73.6 µm and 70.7 to 76.7 µm, respectively, whereas in non-MSGE, this increases up to 81.7 to 92 µm and 86 to 102 µm. The results show that the specimens in MSGE are about 15% smaller than in non-MSGE (Figures 4 and 5). Considering the number of pad-bearing specimens, the percentage observed in MSGE ranges from 3.0% to 32.9%, whereas in non-MSGE, it varies between 43.2% and 52.8%. This indicates a reduced occurrence of pad-bearing specimens in MSGE compared to non-MSGE. There is only one sample from MSGE that, with 47.1% of pads-bearing specimens and 88.1 µm of average equatorial diameter, clusters better with those from non-MSGE. The rest of structural elements measured in *M. mosesii* evidence variations among samples with no clear tendencies or signs of clustering (Supplementary Table 1).

4.b. Inorganic element fixation during cyst stage

The elements assimilated by *M. mosesii* detected with TOF-SIMS spectra are shown in Figure 6. The most striking feature concerns the behaviour of As. This element is commonly detected, with variable intensity, in all but three MSGE samples, but it is absent or shows very low concentration in most of the samples from non-MSGE. Other elements, including Mg, Al, Si, Fe, Zn, Co, Cs, Cr, Ba and Pb, were detected virtually in all TOF-SIMS spectra, but with

https://doi.org/10.1017/S0016756825100034 Published online by Cambridge University Press

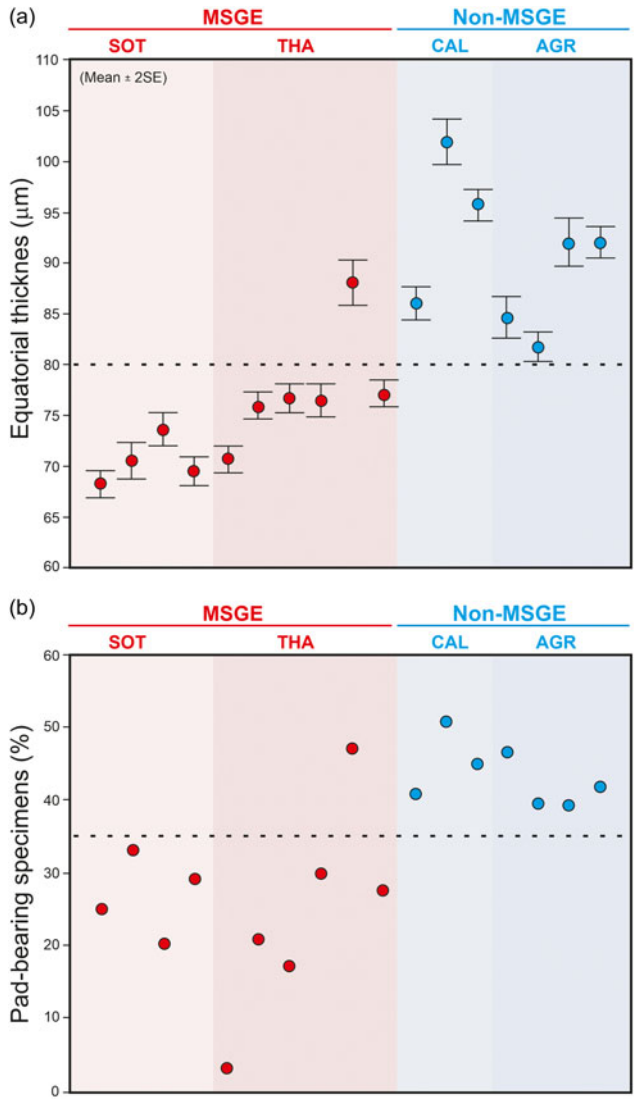

Figure 4. Average equatorial size (a) and percentage of pad-bearing specimens of *M. mosesii* (b) in samples from MSGE and non-MSGE. SOT, Sotiel; THA, Tharsis; CAL, Calañas; AGR, Águila Range.

variable intensities and no differentiation between MSGE and non-MSGE. Of these, Si shows intense peaks in all cases, Co is the element with the highest variability and Ba and Ce depict very similar behaviour, drawing a distribution pattern apparently not related to the environmental differentiation followed in this study. The rest of the elements analyzed, i.e., Cu, Hg, Ce and Cd, were absent, detected randomly or with very low intensity. The elemental chemical TOF-SIMS images (Figure 7) show that the level of enrichment in As, Fe and Al occasionally differs among specimens from a given sample, indicating that these elements were gradually assimilated by *M. mosesii* during cyst growth. Such contrasting occurrences exclude the influence of diagenetically controlled enrichment mechanisms. Other elements, including Si, Mg, Co, Cs and Pb, remain fairly constant in all the specimens of a given sample, suggesting that the enrichment mechanism was in these cases related to a generalized post-depositional process. At the level of specimen, the TOF-SIMS shows no compositional variations across the surface, indicating that the outer wall of *M. mosesii* has a uniform chemical structure and that the elemental enrichment, either at cyst stage or during post-depositional assimilation, was also uniform.

4.3. Seafloor environment reconstruction

Geochemical analysis of the black shales hosting the cysts of *M. mosesii* indicates oxygen-deficient conditions according to Hatch and Leventhal (1992) and Hoffman *et al.* (1998), with the chemocline very close to the sediment-water interface (Jones & Manning, 1994) and no significant differences between MSGE and non-MSGE (Figure 8a and Supplementary Table 2). The alternative use of the U and Mo enrichment factors (Algeo & Tribovillard, 2009;Algeo & Li, 2020) yields similar results (Figure 8b). The absence of covariation between both factors and the consistently low absolute values of Mo_{EF} and U_{EF} for all samples, except for one ($U_{EF} = 7.32$), support the interpretation of generally oxic marine conditions, with the redox chemocline positioned near the water-sediment interface (Algeo & Tribovillard, 2009). For full discussion on redox condition of IPB sulphide-hosting environments see Sáez *et al.* (2011). Although the precise extension of the oxygen-depleted water column is not provided by these geochemical data, the abundance of organic-walled microphytoplankton, including *M. mosesii*, in all samples suggests a vertical zonation pattern with oxygenated water at least in the upper photic zone. Both acritarch cysts and prasinophyte phycomata, the two microphytoplankton groups reported in the studied samples, are generated by the encystment of motile aerobic organisms that, for comparison with modern analogues, require a photic and oxygenated habitat for living (Wong *et al.* 2023).

The comparison of spider-like diagrams for black shales from the two environment sceneries considered in this study shows strong positive anomaly for As and Se in MSGE. Minor anomalies for P, Cu, Zn and Pb are also noticeable (Figure 8c). Analytical values for Cu, Pb and As normalized to TiO^2 are presented in Figure 8d. It shows that all but two samples from non-MSGE form a cluster near the Cu corner, whereas shales from MGSE are dispersed and relatively enriched in As and Pb.

In the IPB, the generation of sulfide deposits was associated with highly efficient hydrothermal systems (Sáez *et al.* 2024). High-temperature hydrothermal mineralizing fluids co-transported reduced sulphur and metals from deeper to near-surface zones. Under this scenario, the occurrence of Cu, As and Pb in MSGE seafloor, along with the other metals that ultimately contributed to the formation of the massive sulphide deposits, would be expected.

In non-polluted marine environments, Cu is generally used as proxy for bioproductivity (Tribovillard *et al.* 2004; Riquier *et al.* 2006), while As and Pb are considered highly poisonous for living organisms (Davies, 1979; Sharma & Sohn, 2009).

5. Discussion

The conjugate analysis of the three techniques employed provides information about the interaction of *M. mosesii* with their hosting environment. Although the morphological variability detected here is linked with the growth trend previously accounted for this species (González, 2009), specimens reported in MSGE are systematically smaller and lighter than those from non-MSGE. Besides, their external wall is enriched in As, a poisoned element more abundant in MSGE than in non-MSGE MSGE that is common in IPB massive sulphide and stockwork mineralization in the form of arsenopyrite and tennantite (Almodóvar *et al.* 2019).

https://doi.org/10.1017/S0016756825100034 Published online by Cambridge University Press

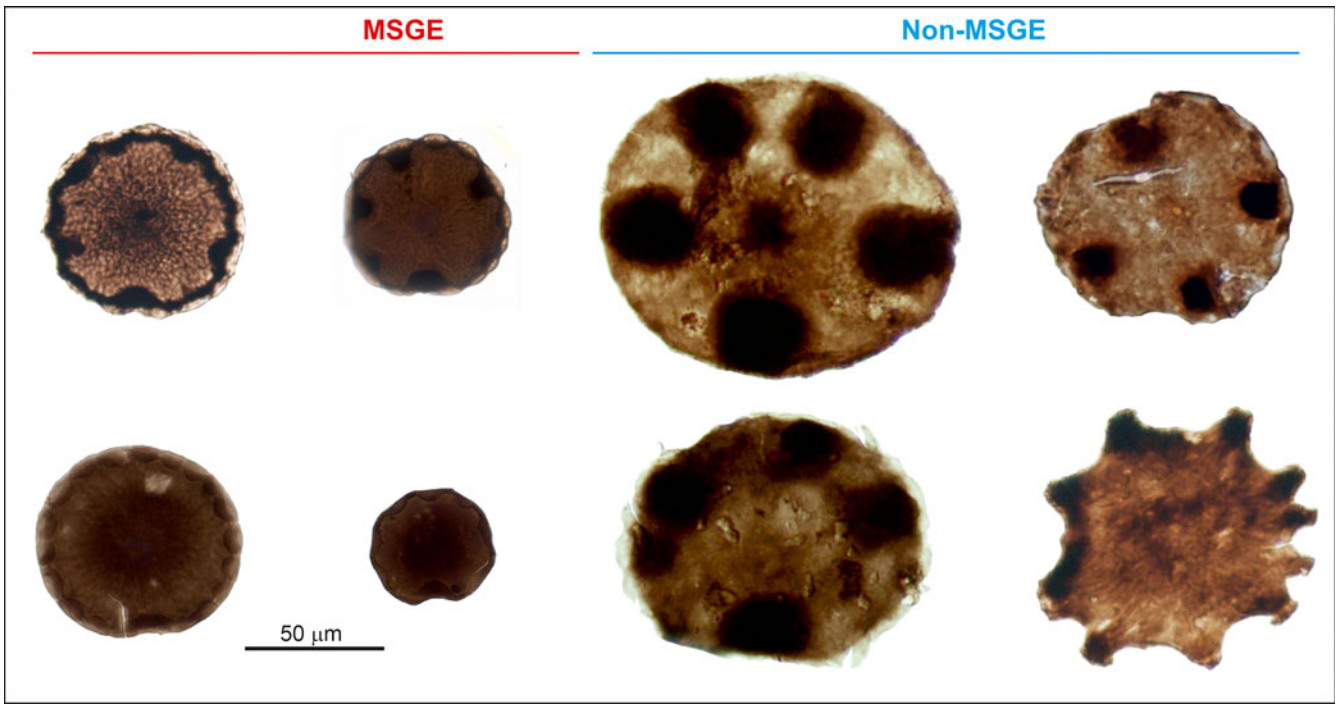

Figure 5. Specimens of *M. mosesii* recovered in MSGE and non-MSGE showing clear differences in equatorial size.

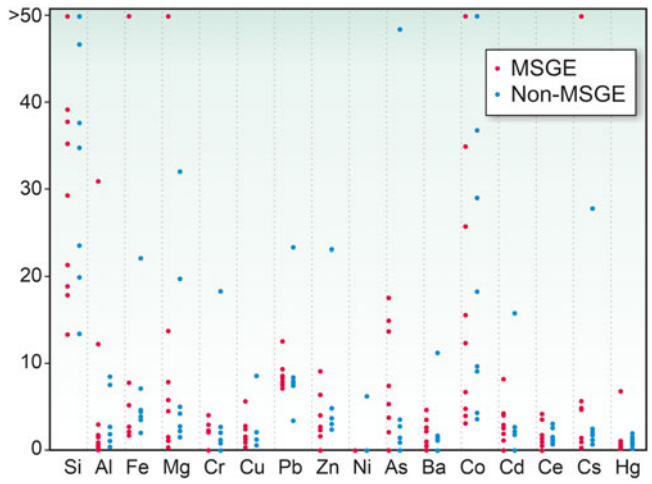

Figure 6. Elements detected in *M. mosesii* from MSGE and non-MSGE based on TOF-SIMS spectra. Vertical scale represents enrichment factor with respect to the holder (adhesive tape). Spectra normalized to PDMS peaks (m/z 147 and 207) identified in the holder tape.

This indicates that cysts of *M. mosesii* sank after encystment, maturating at the bottom of the different sub-basins. There, the disparate environmental conditions conditioned the cyst maturation.

In living, cyst-producing dinoflagellates, the intraspecific morphological variability has been largely associated with changes in temperature, salinity, nutrient levels or pollutants (Dale, 1996; Ellegaard *et al.* 2002, 2017; Pospelova *et al.* 2002, 2005). In the fossil record, morphological perturbations of dinocysts and acritarchs have been also associated with local changes in salinity (Dybkjær, 2004), but more commonly with global factors such as fluctuations in the C cycle (Delabroye *et al.* 2012; Munnecke *et al.* 2012) or expansion of oceanic anoxic events (Vandenbroucke *et al.* 2015). Nevertheless, the variability detected in acritarchs and dinoflagellates, either living or fossil, is understood as the interaction of their parent flagellate cells with the surrounding environment (Kremp *et al.* 2009; Lundholm *et al.* 2011). During the non-flagellate phase, the metabolic activity drastically decreases, remaining, in most cases, at the expense of internal carbohydrate reserves (Binder & Anderson, 1990). Thus, the resting cysts of acritarchs and dinoflagellates virtually operate as closed systems, sensitive to variations in temperature, light and redox conditions (Anderson *et al.* 2005; Brosnahan *et al.* 2020), but not interacting or interacting minimally with their hosting environment.

In the case of living or fossil prasinophytes, studies about intraspecific morphological variations and differential growth rates are very scarce. The available data suggest that, although the morphology of the prasinophytes cyst, called phycomata, can be governed by global climatic factors (Spiridonov *et al.* 2017), it must be also influenced by the environmental conditions prevailing at maturation sites (Boalch & Mommaerts, 1969). There, the substantial phycomata enlargement (Wiebe *et al.* 1974; Parke *et al.* 1978; Colbath, 1983; Knoll *et al.* 1991; Tyson, 1995), which in current prasinophytes can represent an increase of up to 5000 times the size of the precursor flagellate cells (Tappan, 1980), requires of an extracellular energetic source (Pazio, 2016).

On the other hand, the effects of As on modern phytoplankton have been studied in detail. Although with different efficiency, these organisms are capable of bio-uptaking inorganic As, generally as arsenate (III), and subsequently reduce it to arsenite (IV) in order to form more complex and less toxic methylated organic compounds that are then excreted as a detoxification mechanism (Neff, 1997; Yamaoka *et al.* 1999; Goessler *et al.* 1997; Caumette *et al.* 2011; Giovannoni *et al.* 2019). They are even capable of assimilating small proportions of inorganic As. However, when they are exposed to anomalously high As

https://doi.org/10.1017/S0016756825100034 Published online by Cambridge University Press

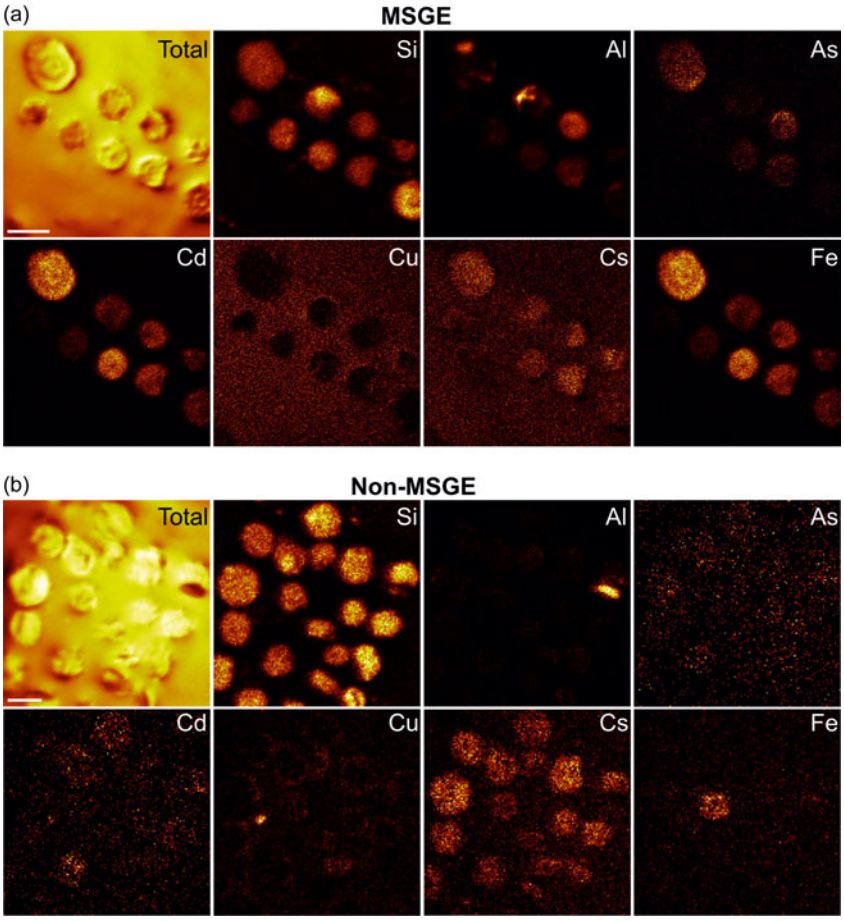

Figure 7. TOF-SIMS chemical images of selected elements detected in specimens of *M. mosesii* from sample THA-4, as representative of MSGE (a) and sample AGR_1, as representative of non-MSGE (b). Scale bars 100 μm.

concentrations, their maturation capacity can be affected and even their lethality increases (Planas & Healey 1978). This behaviour regarding As refers exclusively to non-cyst-forming species or to the flagellate phase of cyst-forming phytoplanktonic organisms. The drastic metabolic reduction in their cyst phase minimizes their element assimilation and their potential infection. This explains the absence of information in the available literature on the effect that As, or any other element, can produce on dinoflagellate and acritarch resting cysts. There are also no studies to our knowledge on the effect of the environment on current prasinophyte phycomata, despite in this case, its huge enlargement suggests metabolic activity beyond the consumption of internal carbohydrate reserves.

In the absence of comparative studies and considering the environmentally induced behaviour of *M. mosesii* here detected, we hypothesize that this species established an anaerobic interchange with the surrounding oxygen-depleted environment during cyst maturation and that As fixation was a by-product of such metabolic process. During maturation, the metabolic activity responsible for As assimilation gradually gained importance. This explains the different As concentrations detected among specimens of a given sample (Figure 7). In non-MSGE, the cysts of *M. mosesii* also contain As, although in minor proportion. This is explained by the ubiquitous occurrence of As in the marine realm, particularly in oxygen-depleted environments (Leventhal, 1991; Bodin *et al.* 2006; Liu & Cai, 2010). When cysts reached an optimum level of maturation, regardless of the level of As accumulated, they moved up in the water column favoured by near-bottom and/or upwelling currents, and finally dispersed their offspring in well-oxygenated near-surface waters. Supporting this hypothesis is the fact that cyst-forming phytoplankton requires oxygenated environments for excystment and germination (Anderson *et al.* 1987; Kremp & Anderson, 2000; Ellegaard *et al.* 2017), and that specimens of *M. mosesii* having excystment structures, i.e., those that resuspended to the photic zone and settled on the bottom again, are in much smaller proportion than non-excysted cysts. The equatorial solid pads in this species (Figures 3 and 5) could have been used as energy storage devices or as structures within a floating/sinking system. Their consumption or detachment, joined with the development and progressive enlargement of the equatorial, hollow, transparent bladders that characterize the latest growth stages in this species (González, 2009), favoured the final resuspension of mature cysts. The elevated concentration of As in MSGE decreased the metabolic interchange with the surrounding medium or accelerated the cysts maturation, and with it their resuspension, in order to attenuate, or diminish, the exposure to a hostile environment. The reduced equatorial diameter and small amount of pad-bearing cysts were the consequences of this process.

The common to elevated occurrence of *M. mosesii* cysts in most MSGE samples suggests that such adaptative mechanism was effective. However, the quantitative analysis of the relative proportion of acritarchs, prasinophyte phycomata and *M. mosesii* specimens (Figure 9) shows that MSGE samples are mostly dominated by acritarchs whereas non-MSGE samples are mostly

https://doi.org/10.1017/S0016756825100034 Published online by Cambridge University Press

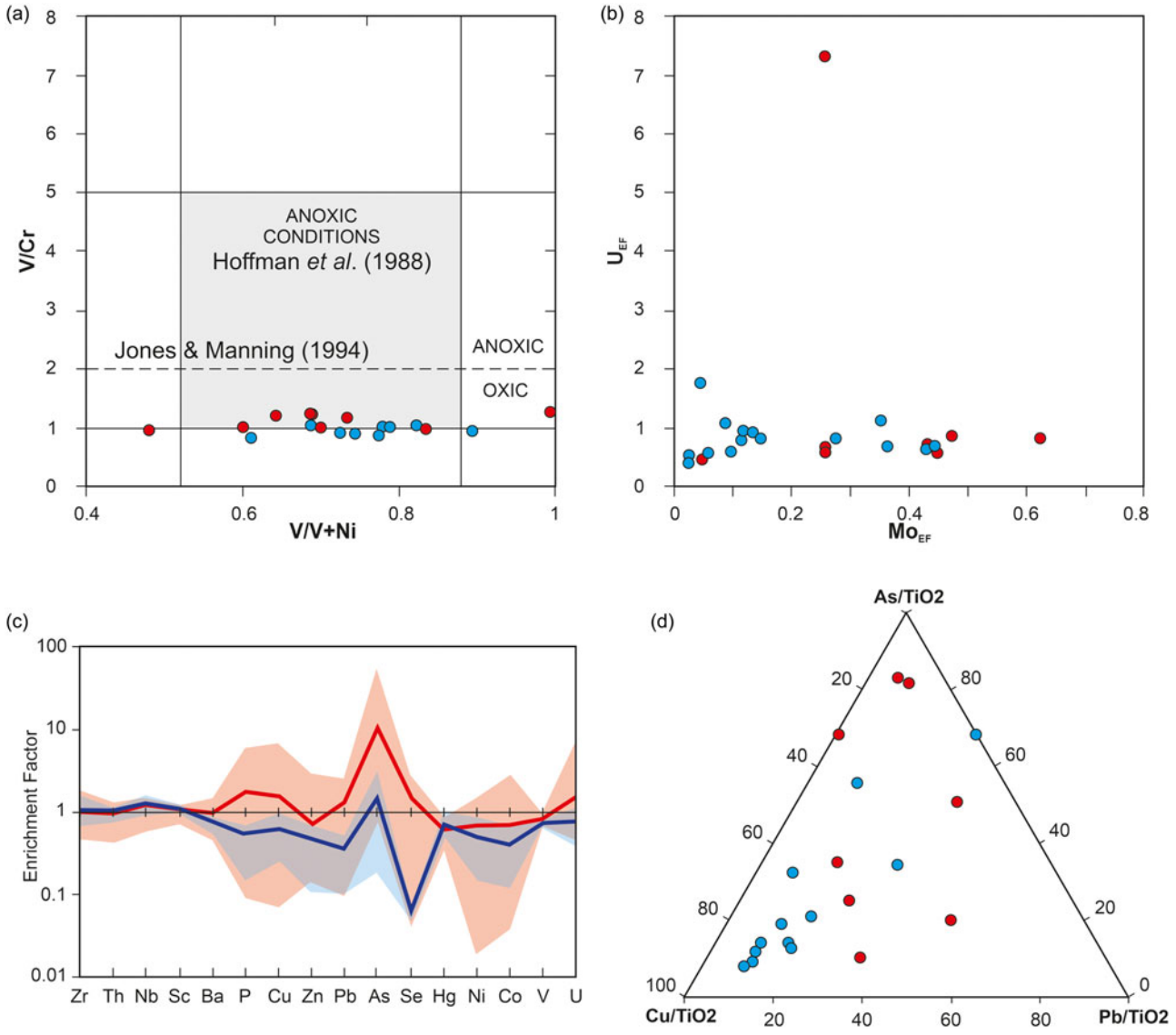

Figure 8. (a) Bivariate plot of the black shale samples from MSGE (red circles) and non-MSGE (blue circles) in the diagram V/Cr *vs* V/(V+Ni). Limits of environmental conditions after the Hoffman *et al.* (1998) and Jones and Manning (1994); (b) Diagram U_{EF} vs Mo_{EF}; (c) PAAS-normalized spider-like diagrams for maximum, minimum and average values (bold lines) of black shale samples. Red and blue lines represent samples from MSGE and non-MSGE, respectively; (d) Ternary diagram showing the relative proportion of Cu-As-Pb normalized to TiO_2. Red and blue circles for MSGE and non-MSGE, respectively.

dominated by M. *mosesii*. In addition, the percentage of this species is most fluctuating in MSGE than in non-MSGE samples. This means that, although *M. mosesii* can be adapted to pollutant conditions, they germinate more abundantly in non-stressed environments.

Regardless of whether cyst size reduction in *M. mosesii* is an adaptive mechanism or a limitation resulting from growing under hostile conditions, a causal relationship between cyst size and hosting environment is clearly established. This means that, in the IPB, the biometric analysis of *M. mosesii* specimens provides an effective tool for distinguishing late Devonian black shales sequences associated with massive sulphides from barren sequences (without massive sulphides). To date, the contribution of palynology to the study of the IPB basin has primarily focused on the detailed biostratigraphic analysis of shale sequences belonging to its three chronostratigraphic units, with special emphasis on the VSC sequences hosting the massive sulphides and the coeval underlaying PQ sequences cut by stockwork type mineralization (i.e., Pereira *et al.* 1996, 2004, 2021, 2023; González *et al.* 2002, González *et al.*, 2006; Mendes *et al.* 2020, 2024; Sáez *et al.* 2007). The present study goes a step further by aiding in the identification of potential targets for sulphide exploration in the region, paying special attention to the massive sulphide and stockwork-type mineralization hosted by black shales.

Finally, in terms of suprageneric affiliation, *M. mosesii*, and for extension the genus *Maranhites* (Brito 1965) emend González 2009, cannot be unquestionably assigned to the Prasinophyceae Class due to the absence of morphologically comparable extant counterparts. However, its preference for oxygen-depleted environments and its active metabolism during the cyst phase, unreported in living and fossils acritarch and dinoflagellates, reinforces the hypothesis by Tappan (1980), Colbath and Grenfell (1995) and Lé Hérissé *et al.* (2009) by which *Maranhites* may have prasinophyte affinity.

https://doi.org/10.1017/S0016756825100034 Published online by Cambridge University Press

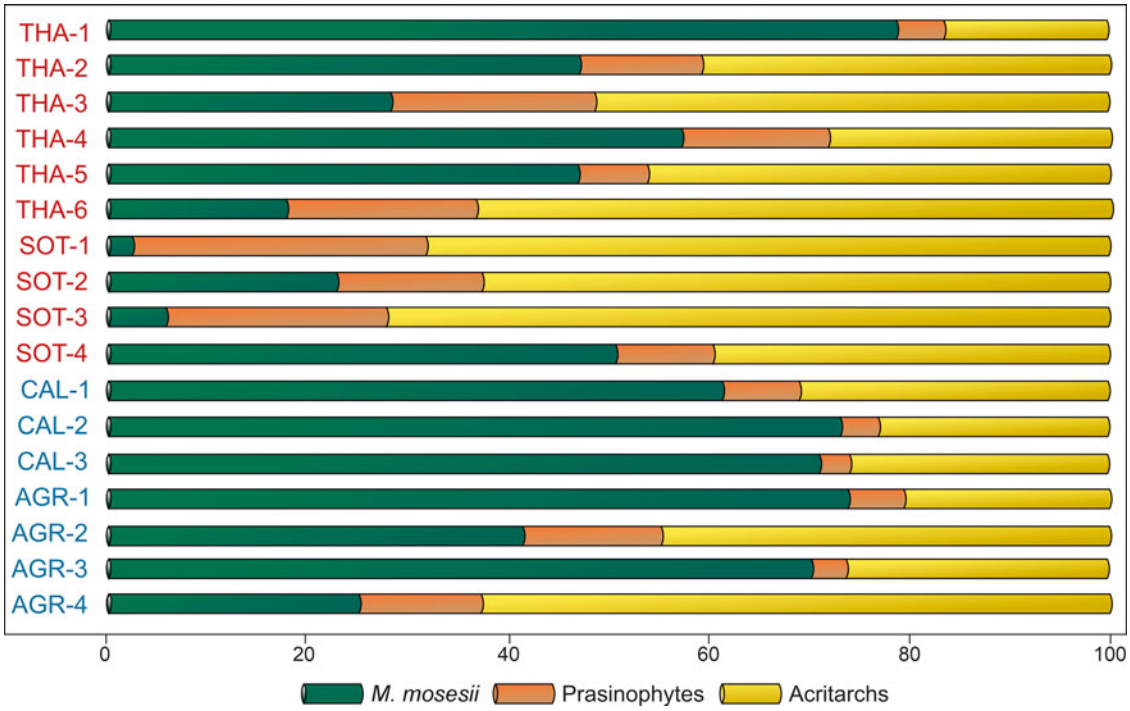

Figure 9. Quantitative analysis of the phytoplankton recovered in the studied samples (in percentages). Samples in red from MSGE. Samples in blue from non-MSGE. Location of samples is indicated in Figure 1.

6. Conclusions

The latemost Devonian palynological assemblages from the IPB are unusually enriched in the microphytoplankton species *M. mosesii*. This species is abundant in both MSG and non-MSGE environments. The geochemistry of the shales recovered in MSG and non-MSGE environments indicates that both habitats are characterized by oxygen-depleted seafloor conditions and that most of the MSGE samples were enriched in pollutants, including As and Pb. The specimens of *M. mosesii* reported in MSGE were smaller and lighter than those from non-MSGE. Besides, the MSGE specimens depicted anomalous high values of As on their outer walls. This indicates that cysts of this species sank after encystment and were affected during maturation by disparate seafloor environmental conditions. The abundance of *M. mosesii* in both groups of environments also suggests that this species implemented during its growing cyst phase a successful adaptive mechanism to oxygen-depleted conditions that might involve anaerobic metabolic interchange with the surrounding media and high level of tolerance to stressors.

The multi-analytical analysis employed in this study, which involves (1) biometry of microphytoplankton fossils, (2) TOFSIMS imaging and surface analysis of selected specimens and (3) host rock geochemistry, has resulted useful for unravelling the interrelation of metabolically active cysts with its surrounding seafloor environment. The causal relationship established between cyst size and environmental conditions allows the biometry of *M. mosesii* to be viewed as a promising prospective vector for massive sulphide and stockwork-type deposits in the IPB.

Supplementary material. For supplementary material/s referred to in this article, please visit https://doi.org/10.1017/S0016756825100034

Acknowledgements. The original manuscript was improved thanks to the suggestions and comments of five anonymous reviewers.

Financial support. This research was funded by the CICYT (Spain) Research Project CGL2016-79204-R and the Research Group THARSIS RNM 198-PAI (Junta de Andalucía).

References

Albardeiro L, Morais I, Matos JX, Solá R, Salgueiro R, Pereira Z, Mendes M, Batista MJ, De Oliveira D, Díez-Montes A, Inverno C, Pacheco N and Araújo V (2023) Time-space evolution of Iberian Pyrite Belt igneous activity: volcanic and plutonic lineaments, geochronology, ore horizons and stratigraphic constraints. *Gondwana Research* **121**, 235–58. https://doi.org/10.1016/j.gr.2023.05.004

Albardeiro L, Matos JX, Mendes M, Solá R, Pereira Z, Morais I, Salgueiro R, Pacheco N, Araújo V and Oliveira JT (2020) Geological correlation of Neves-Corvo Mine and Pomarão Antiform sequences (Iberian Pyrite Belt, Portugal). *Comunicações Geológicas LNEG* **107**, 111–32.

Algeo TJ and Li C (2020) Redox classification and calibration of redox thresholds in sedimentary systems. *Geochimica et Cosmochimica Acta* **287**, 8–26. https://doi.org/10.1016/j.gca.2020.01.055

Algeo TJ and Tribovillard N (2009) Environmental analysis of paleoceanographic systems based on molybdenum–uranium covariation. *Chemical Geology* **268**, 211–25. https://doi.org/10.1016/j.chemgeo.2009.09.001

Almodóvar GR, Yesares L, Sáez R, Toscano M, González F and Pons JM (2019) Massive sulfide ores in the Iberian Pyrite Belt: mineralogical and textural evolution. *Minerals* **9**, 653. https://doi.org/10.3390/min9110653

Anderson DM, Stock CA, Keafer BA, Nelson AB, Thompson B, McGillicuddy DJ. Jr, Keller M, Matrai PA and Martin J (2005) *Alexandrium fundyense* cyst dynamics in the Gulf of Maine. *Deep-Sea Research II* **52**, 2522–42. https://doi.org/10.1016/j.dsr2.2005.06.01

Anderson DM, Taylor CD and Armbrust EV (1987) The effects of darkness and anaerobiosis on dinoflagellate cyst germination. *Limnology and Oceanography* **32**, 340–51. https://doi.org/10.4319/lo.1987.32.2.0340

Barrie CT, Amelin Y and Pascual E (2002) U-Pb geochronology of VMS mineralization in the Iberian Pyrite Belt. *Mineralium Deposita* **37**, 684–703. https://doi.org/10.1007/s00126-002-0302-7

Binder BJ and Anderson DM (1990) Biochemical composition and metabolic activity of *Scrippsiella trochoidea* (Dinophyceae) resting cysts. *Journal of Phycology* **26**, 289–98. https://doi.org/10.1111/j.0022-3646.1990.00289.x

Boalch GT and Mommaerts JP (1969) A new punctate species of *Halosphaera*. *Journal of the Marine Biological Association of the United Kingdom* **49**, 129–39. https://doi.org/10.1017/S0025315400046464

Bodin S, Godet A, Matera V, Steinmann P, Vermeulen J, Gardin S, Adatte T, Coccioni R and Föllmi KB (2006) Enrichment of redox-sensitive trace metals (U, V, Mo, As) associated with the late Hauterivian Faraoni oceanic anoxic event. *International Journal of Earth Sciences* **96**, 327–41. https://doi.org/10.1007/s00531-006-0091-9

Boogaard M van den (1963) Conodonts of Upper Devonian and Lower Carboniferous age from southern Portugal. *Geologie Mijnbouw* **42**, 248–59.

Boogaard M van den and Schermerhörn LJG (1981) Conodont faunas from Portugal and southwestern Spain. Part 4. A Famennian conodont fauna near Nerva (Río Tinto). *Scripta Geologica* **56**, 1–14.

Brosnahan ML, Fischer AD, López CB, Moore SK and Anderson DM (2020) Cyst-forming dinoflagellates in a warming climate. *Harmful Algae* **91**, 101728. https://doi.org/10.1016/j.hal.2019.101728

Caumette G, Koch I, Estrada E and Reimer KJ (2011) Arsenic speciation in plankton organisms from contaminated lakes: transformations at the base of the freshwater food chain. *Environmental Science and Technology* **45**, 9917–23. https://doi.org/10.1021/es2025092

Colbath GK (1983) Fossil prasinophycean phycomata (Chlorophyta) from the Silurian Bainbridge Formation, Missouri, U.S.A. *Phycologia* **22**, 249–65. https://doi.org/10.2216/i0031-8884-22-3-249.1

Colbath GK and Grenfell HR (1995) Review of biological affinities of Paleozoic acid-resistant, organic-walled eukaryotic algal microfossils (including "acritarchs"). *Review of Palaeobotany and Palynology* **86**, 287–14. https://doi.org/10.1016/0034-6667(94)00148-D

Dale B (1996) Dinoflagellate cyst ecology: Modelling and geological applications. In *Palynology: Principles and Applications* (eds J Jansonius and DC McGregor), pp. 1249–1275. Dallas: American Association of Stratigraphic Palynologists Foundation, 2.

Davies AG (1979) Pollution studies with marine plankton: Part II. Heavy metals. *Advances in Marine Biology* **15**, 381–508. https://doi.org/10.1016/S0065-2881(08)60408-3

Delabroye A, Munnecke A, Servais T, Vandenbroucke TRA and Vecoli M (2012) Abnormal forms of acritarchs (phytoplankton) in the upper Hirnantian (Upper Ordovician) of Anticosti Island, Canada. *Review of Palaeobotany and Palynology* **173**, 46–56. https://doi.org/10.1016/j.revpalbo.2011.10.010

Dunning GR, Díez Montes A, Matas J, Martín Parra LM, Almarza J and Donaire M (2002) Geocronología U/Pb del vulcanismo ácido y granitoides de la Faja Pirítica Ibérica (Zona Surportuguesa). *Geogaceta* **32**, 127–30.

Dybkjær K (2004) Morphological and abundance variations in *Homotryblium* cyst assemblages related to depositional environments; uppermost Oligocene–Lower Miocene, Jylland, Denmark. *Palaeogeography, Palaeoclimatology, Palaeoecology* **206**, 41–58. https://doi.org/10.1016/j.palaeo.2003.12.021

Ellegaard M, Dale B, Mertens K, Pospelova V and Ribeiro S (2017) Dinoflagellate cysts as proxies for Holocene environmental change in estuaries: diversity, abundance and morphology. In *Applications of Palaeoenvironmental Techniques in Estuarine Studies* (eds K Weckström, K Saunders, KP Gell and C Skilbeck), pp. 295–312. Developments in Palaeoenvironmental Research, Berlin: Springer, 20. https://doi.org/10.1007/978-94-024-0990-1_12

Ellegaard M, Lewis J and Harding I (2002) Cyst-theca relationship, life cycle, and effects of temperature and salinity on the cyst morphology of *Gonyaulax baltica* sp. nov. (Dinophyceae) from the Baltic Sea area. *Journal of Phycology* **38**, 775–89. https://doi.org/10.1046/j.1529-8817.2002.01062.x

Giovannoni SJ, Halsey KH, Saw, J, Muslin O, Suffridge CP, Sun J, Lee C, Moore ER, Temperton B and Noell SE (2019) A parasitic arsenic cycle that shuttles energy from phytoplankton to heterotrophic bacterioplankton. *mBio* **10**, e00246–19. https://doi.org/10.1128/mbio.00246-19

Goessler W, Lintschinger J, Szakova J, Mader P, Kopecky J, Douch J and Irgolic KJ (1997) *Chlorella* sp. and arsenic compounds: an attempt to prepare an algal reference material for arsenic compounds. *Applied Organometallic Chemistry* **11**, 57–66. https://doi.org/10.1002/(SICI)1099-0739(199701)11:1<57::AID-AOC540>3.0.CO;2-J

González F (2009) Reappraisal of the organic-walled microphytoplankton genus *Maranhites*: morphology, excystment, and speciation. *Review of Palaeobotany and Palynology* **154**, 6–21. https://doi.org/10.1016/j.revpalbo.2008.11.004

González F, Moreno C, López MJ, Dino R and Antonioli L (2003) Palinoestratigrafía del Grupo Pizarroso-Cuarcítico del sector más oriental de la Faja Pirítica Ibérica, SO de España. *Revista Española de Micropaleontología* **36**, 279–304.

González F, Moreno C and Playford G (2005b) Upper Devonian biostratigraphy of the Iberian Pyrite Belt, southwest Spain. Part One: miospores. *Paläontologische Zeitschrift B* **273**, 1–51. https://doi.org/10.1127/palb/273/2005/1

González F, Moreno C and Sáez R (2002) Ore genesis age of the Tharsis Mining District (Iberian Pyrite Belt): a palynological approach. *Journal of the Geological Society of London* **159**, 229–32. https://doi.org/10.1144/0016-764901-142

González F, Moreno C and Santos A (2006) The massive sulfide event in the Iberian Pyrite Belt: confirmatory evidence from the Sotiel-Coronada mine. *Geological Magazine* **143**, 821–27. https://doi.org/10.1017/S0016756806002573

González F, Playford G and Moreno C (2005a) Upper Devonian biostratigraphy of the Iberian Pyrite Belt, southwest Spain. Part Two: organic-walled microphytoplankton. *Palaeontographica Abteilung B* **273**, 53–86. https://doi.org/10.1127/palb/273/2005/53

Hatch JR and Leventhal JS (1992) Relationship between inferred oxidation potential of the depositional environment and geochemistry of the Upper Pennsylvanian (Missourian) Stark Shale Member of the Dennis Limestone, Wabaunsee County, Kansas, U.S.A. *Chemical Geology* **99**, 65–82. https://doi.org/10.1016/0009-2541(92)90031-y

Hoffman DL, Akgeo TJ, Maynard B, Joachimski MM, Hower JC and Jaminski J (1998) Regional stratigraphic variation in bottom water anoxia in offshore core shales of Upper Pennsylvanian cyclothems from Eastern Midcontinent Shelf (Kansas), USA. In *Shales and Mudstones* (eds J Schieber, W Zimmerle and P Sethi), pp. 243–269. Stuttgart: E. Schweizerbart'sche Verlagsbuchhandlung.

Jones B and Manning DAC (1994) Comparison of geochemical indices used for interpretation of paleoredox conditions in ancient mudstones. *Chemical Geology* **111**, 111–29. https://doi.org/10.1016/0009-2541(94)90085-X

Knoll AH, Swett K and Mark J (1991) Paleobiology of a Neoproterozoic tidal flat/lagoonal complex: The Draken Conglomerate Formation, Spitsbergen. *Journal of Paleontology* **65**, 531–70. https://doi.org/10.1017/s0022336000030663

Kremp A and Anderson DM (2000) Factors regulating germination of resting cysts of the spring bloom dinoflagellate *Scrippsiella hangoei* from the northern Baltic Sea. *Journal of Plankton Research* **22**, 1311–27. https://doi.org/10.1093/plankt/22.7.1311

Kremp A, Rengefors K and Montresor M (2009) Species-specific encystment patterns in three Baltic cold-water dinoflagellates: the role of multiple cues in resting cyst formation. *Limnology and Oceanography* **54**, 1125–38. https://doi.org/10.4319/lo.2009.54.4.1125

Le Hérissé A, Dorning KJ, Mullins GL and Wicander R (2009) Global patterns of organic-walled phytoplankton biodiversity during the late Silurian to earliest Devonian. *Palynology* **33**, 25–75. https://doi.org/10.1080/01916122.2009.9989665

Leistel JM, Marcoux E and Deschamps Y (1998) Chert in the Iberian Pyrite Belt. *Mineralium Deposita* **33**, 59–81.

Leistel JM, Marcoux E, Thiéblemont D, Quesada C, Sánchez A, Almodóvar GR, Pascual E and Sáez R (1998) The volcanic-hosted massive sulfide deposits of the Iberian Pyrite Belt: review and preface to the thematic issue. *Mineralium Deposita* **33**, 2–30. https://doi.org/10.1007/s001260050130

Leventhal JS (1991) Comparison of organic geochemistry and metal enrichment in two black shales: Cambrian Alum Shale of Sweden and Devonian Chattanooga Shale of the United States. *Mineralium Deposita* **26**, 104–12. https://doi.org/10.1007/bf00195256

Liu G and Cai Y (2010) Complexation of arsenite with dissolved organic matter: conditional distribution coefficients and apparent stability constants. *Chemosphere* **81**, 890–96. https://doi.org/10.1016/j.chemosphere.2010.08.002

Lundholm N, Ribeiro S, Andersen TJ, Koch T, Godhe A, Ekelund F and Ellegaard M (2011) Buried alive: germination of up to a century-old marine protist resting stages. *Phycologia* **50**, 629–40. https://doi.org/10.2216/11-16.1

Martín-Izard A, Arias D, Arias M, Gumiel P, Sanderson DJ, Castañón C and Sánchez J (2017) Ore deposit types and tectonic evolution of the Iberian Pyrite Belt: from transtensional basins and magmatism to transpression and inversion tectonics. *Ore Geology Reviews* **79**, 254–67. https://doi.org/10.1016/j.oregeorev.2016.05.011

Matos JX, Pereira Z, Rosa C and Oliveira JT (2014) High resolution stratigraphy of the Phyllite-Quartzite Group in the northwest region of the Iberian Pyrite Belt, Portugal. *Comunicações Geológicas* **101**, 489–93.

Mendes M, Pereira Z, Matos J, Albardeiro L, Morais I and Araújo V (2024) Late Famennian (latest Strunian) palynomorph assemblages and their role in the Neves Formation depositional environment—The Neves-Corvo mine case study (Iberian Pyrite Belt, Portugal). *Revue de Micropaléontologie* **84**, 2–14. https://doi.org/10.1016/j.revmic.2024.100805

Mendes M, Pereira Z, Matos JX, Albardeiro L, Morais I, Solá R, Salgueiro R, Pacheco N, Araújo V, Inverno C and Oliveira JT (2020) New insights on the middle Givetian/middle Frasnian palynofloras from the Phyllite-Quartzite Formation in the Neves-Corvo mine region (Iberian Pyrite Belt, Portugal). *Revue de Micropaléontologie* **68**, 100447. https://doi.org/10.1016/j.revmic.2020.100447

Moreno C (1993) Postvolcanic Paleozoic of the Iberian Pyrite Belt: an example of basin morphologic control on sediment distribution in a turbidite basin. *Journal of Sedimentary Petrology* **63**, 1118–1128. https://doi.org/10.1306/D4267CBC-2B26-11D7-8648000102C1865D

Moreno C, González F and Sáez R (2003) Inicio del vulcanismo en el sector de Calañas (Faja Pirítica Ibérica): caracterización y datación. *Geogaceta* **33**, 59–62.

Moreno C and González F (2004) Estratigrafía de la Zona Surportuguesa. In *Geología de España* (ed JA Vera), pp. 201–205. Sociedad Geológica de España and Instituto Geológico y Minero de España.

Moreno C and Sequeiros L (1989) The Basal Shaly Formation of the Iberian Pyrite Belt (South-Portuguese Zone): early Carboniferous bituminous deposits. *Palaeogeography, Palaeoclimatology, Palaeoecology* **73**, 233–41. https://doi.org/10.1016/0031-0182(89)90006-0

Moreno C, Sierra S and Sáez R (1996) Evidence for catastrophism at the Famennian–Dinantian boundary in the Iberian Pyrite Belt: recent advances. In *Lower Carboniferous Geology* (P Strogen, D Somerville and GL Jones), pp. 153–162. Geological Society Special Publications 107. https://doi.org/10.1144/GSL.SP.1996.107.01.12

Munnecke A, Delabroye A, Servais T, Vandenbroucke TRA and Vecoli M (2012) Systematic occurrences of malformed (teratological) acritarchs in the run-up of Early Palaeozoic δ13C isotope excursions. *Palaeogeography, Palaeoclimatology, Palaeoecology* **367–368**, 137–46. https://doi.org/10.1016/j.palaeo.2012.02.029

Neff JM (1997) Ecotoxicology of arsenic in the marine environment. *Environmental Toxicology and Chemistry* **16**, 917–27. https://doi.org/10.1002/etc.5620160511

Oliveira JT (1990) South Portuguese Zone: stratigraphy and synsedimentary tectonism. In *Pre-Mesozoic Geology of Iberia* (RD Dallmeyer and E Martínez García), pp. 333–347. Berlin: Springer-Verlag.

Oliveira JT, Pereira Z, Carvalho P, Pacheco N and Korn P (2004) Stratigraphy of the tectonically imbricated lithological succession of the Neves Corvo mine area, IPB, Portugal. *Mineralium Deposita* **39**, 422–36 https://doi.org/10.1007/s00126-004-0415-2

Oliveira JT, Quesada C, Pereira Z, Matos JX, Solá AR, Rosa D, Albardeiro L, Díez-Montes A, Morais I, Inverno C, Rosa C and Relvas J (2019) South Portuguese terrane: a continental affinity exotic unit. In *The Geology of Iberia: A Geodynamic Approach* (eds C Quesada and JT Oliveira), 2, pp. 173–206. New York: Springer. https://doi.org/10.1007/978-3-030-10519-8_6

Oliveira JT, Rosa C, Rosa D, Pereira Z, Matos JX, Inverno C and Andersen T (2013) Geology of the Neves-Corvo antiform, Iberian Pyrite Belt, Portugal: new insights from physical volcanology, palynostratigraphy and isotope geochronology studies. *Mineralium Deposita* **48**, 749–66. https://doi.org/10.1007/s00126-012-0453-0

Parke M, Boalch GT, Jowett R and Harbour DS (1978) The genus *Pterosperma* (Prasinophyceae): species with a single equatorial ala. *Journal of the Marine Biological Association of the United Kingdom* **58**, 239–76. https://doi.org/10.1017/s0025315400024528

Pazio M (2016) The life cycle and developmental phases of Cambrian–Ordovician organic-walled microfossils from Kolguev Island, Arctic Russia. *Examensarbete vid Institutionen för geovetenskaper*. Department of Earth Sciences, Uppsala University, 60 p.

Pereira Z, Matos JX, Mendes M, Solá R, Albardeiro L, Morais I, Araújo V, Pacheco N and Oliveira JT (2023) Biostratigraphic and structural research in the Guedelhinha–Lançadoiras–Algaré sector in the context of the geology of the Neves–Corvo mine region, Iberian Pyrite Belt. *Geobios* **80**, 55–71. https://doi.org/10.1016/j.geobios.2023.06.004

Pereira, Z, Matos JX, Solá AR, Batista MJ, Salgueiro R, Rosa C, Albardeiro L, Mendes M, Morais I, de Oliveira D, Pacheco N, Araújo V, Castelo Branco JM, Neto R, Lains Amaral J, Inverno C and Oliveira JT (2021) Geology of the recently discovered massive and stockwork sulphide mineralization at Semblana, Rosa Magra and Monte Branco, Neves–Corvo mine region, Iberian Pyrite Belt, Portugal. *Geological Magazine* **158**, 1253–68. https://doi.org/10.1017/S0016756820001284

Pereira Z and Pacheco N (2004) A case of applied palynology: dating the lithological succession of the Neves Corvo Mine, Iberian Pyrite Belt, Portugal. *XVth International Congress on Carboniferous and Permian Stratigraphy, Utrecht. Abstracts Book*, 397–401.

Pereira Z, Sáez R, Pons JM, Oliveira JT and Moreno C (1996) Edad devónica (Struniense) de las mineralizaciones de Aznalcóllar (Faja Pirítica Ibérica) en base a palinología. *Geogaceta* **20**, 1609–12.

Pinedo Vara I (1963) *Piritas de Huelva*. Ed. Summa, Madrid, 1003 p.

Planas D and Healey FP (1978) Effects of arsenate on growth and phosphorus metabolism of phytoplankton. *Journal of Phycology* **14**, 337–41. https://doi.org/10.1111/j.1529-8817.1978.tb00309.x

Pospelova V, Chmura GL, Boothman WS and Latimer JS (2002) Dinoflagellate cyst records and human disturbance in two neighboring estuaries, New Bedford Harbor and Apponagansett Bay, Massachusetts (USA). *Science of the Total Environment* **298**, 81–102. https://doi.org/10.1016/S0048-9697(02)00195-X

Pospelova V, Chmura GL, Boothman WS and Latimer JS (2005) Spatial distribution of modern dinoflagellate cysts in polluted estuarine sediments from Buzzards Bay (Massachusetts, USA) embayments. *Marine Ecology Progress Series* **292**, 23–40. https://doi.org/10.3354/meps292023

Riquier L, Tribovillard N, Averbuch O, Devleeschouwer X and Riboulleau A (2006) The Late Frasnian Kellwasser horizons of the Harz Mountains (Germany): two oxygen-deficient periods resulting from different mechanisms. *Chemical Geology* **233**, 137–55. https://doi.org/10.1016/j.chemgeo.2006.02.021

Sáez R, Almodóvar GR and Barriga FJAS (1997) Mineral exploration in the Iberian Pyrite Belt. *SGA News* **3**, 7–11.

Sáez R, Almodóvar GR and Pascual E (1996) Geological constraints on massive sulphide genesis in the Iberian Pyrite Belt. *Ore Geology Reviews* **11**, 429–51. https://doi.org/10.1016/S0169-1368(96)00012-1

Sáez R, González F, Donaire T, Toscano M, Yesares L, Almodóvar GR and Moreno C (2024) Updating geological information about the metallogenesis of the Iberian Pyrite Belt. *Minerals* **14**, 860. https://doi.10.3390/min14090860

Sáez R and Moreno C (1997) Geology of the Puebla de Guzmán anticlinorium. In *Geology and VMS Deposits of the Iberian Pyrite Belt* (eds FJAS Barriga and D Carvalho), Guidebook Series 27, pp. 131–6. Littleton: Society of Economic Geologists.

Sáez R, Moreno C and González F (2008) Synchronous deposition of massive sulphide deposits in the Iberian Pyrite Belt: new data from Las Herrerías and La Torerera ore-bodies. *Comptes Rendus Geoscience* **340**, 829–39. https://doi.org/10.1016/j.crte.2008.08.002

Sáez R, Moreno C, González F and Almodóvar GR (2011) Black shales and massive sulfide deposits: causal or casual relationships? Insights from

Rammelsberg, Tharsis, and Draa Sfar. *Mineralium Deposita* **46**, 585–614. https://doi.org/10.1007/s00126-010-0311-x

Sáez R, Pascual E, Toscano M and Almodóvar GR (1999) The Iberian type of volcano-sedimentary massive sulfide deposits. *Mineralium Deposita* **34**, 549–70. https://doi.org/10.1007/s001260050220

Schermerhörn LJ (1971) An outline stratigraphy of the Iberian Pyrite Belt. *Boletín Geológico y Minero* **8**, 239–68.

Sharma VK and Sohn M (2009) Aquatic arsenic: toxicity, speciation, transformations, and remediation. *Environmental International* **35**, 743–59. https://doi.org/10.1016/j.envint.2009.01.005

Silva JB, Oliveira JT and Ribeiro A (1990) South-Portuguese Zone: structural outline. In *Pre-Mesozoic Geology of Iberia* (eds RD Dallmeyer and E Martínez García), pp. 348–362. Berlin: Springer-Verlag.

Soriano C and Casas JM (2002) Variscan tectonics in the Iberian Pyrite Belt, South Portuguese Zone. *International Journal of Earth Sciences* **91**, 882–96. https://doi.org/10.1007/s00531-001-0253-8

Spiridonov A, Venckutë-Aleksienë A and Radzevičius S (2017) Cyst size trends in the genus Leiosphaeridia across the Mulde (lower Silurian) biogeochemical event. *Bulletin of Geosciences* **92**, 391–404.

Streel M, Higgs K, Loboziak S, Riegel W and Steemans P (1987) Spore stratigraphy and correlation with faunas and floras in the type marine Devonian of the Ardenne–Rhenish regions. *Review of Palaeobotany and Palynology* **50**, 211–29. https://doi.org/10.1016/0034-667(87)90001-7

Tappan H (1980) *The Paleobiology of Plant Protists*. New York: Freeman and Co, 1028 p.

Taylor TN, Taylor EL and Krings M (2009) *Paleobotany: The Biology and Evolution of Fossil Plants*, 2nd ed. Amsterdam: Elsevier, 1230 p.

Teyssèdre B (2006) Are the green algae (phylum Viridiplantae) two billion years old? *Carnets de Géologie* 2006/03. https://doi.org/10.4267/2042/5836

Tornos F, Barriga F, Marcoux E, Pascual E, Pons JM, Relvas J and Velasco F (2000) The Iberian Pyrite Belt. In *Database on Global VMS Districts* (eds RR Large and DJ Blundell), pp. 19–52. CODES-GEODE.

Tribovillard N, Riboulleau A, Lyons T and Baudin F (2004) Enhanced trapping of molybdenum by sulfurized organic matter of marine origin as recorded by various Mesozoic formations. *Chemical Geology* **213**, 385–401. https://doi.org/10.1016/j.chemgeo.2004.08.011

Tyson RV (1995) *Sedimentary Organic Matter: Organic Facies and Palynofacies*. London: Chapman and Hall, 615 p.

Vandenbroucke TRA, Emsbo P, Munnecke A, Nuns N, Duponchel L, Lepot K, Quijada M, Paris F, Servais T and Kiessling W (2015) Metal-induced malformations in early Palaeozoic plankton are harbingers of mass extinction. *Nature Communications* **6**, 7966. https://doi.org/10.1038/ncomms8966

Wiebe PH, Remsen CC and Vaccaro RF (1974) *Halosphaera viridis* in the Mediterranean Sea: size range, vertical distribution, and potential energy source for deep-sea benthos. *Deep-Sea Research and Oceanographic Abstracts* **21**, 657–67. https://doi.org/10.1016/0011-7471(74)90050-3

Wong JCY, Raven JA, Aldunate M, Silva S, Gaitán-Espitia JD, Vargas CA, Ulloa O and Von Dassow P (2023) Do phytoplankton require oxygen to survive? A hypothesis and model synthesis from oxygen minimum zones. *Limnology and Oceanography* **68**, 1417–37. https://doi.org/10.1002/lno.12367

Wood GD, Gabriel AM and Lawson JC (1996) Palynological techniques—Processing and microscopy. In *Palynology: Principles and Applications* (eds J Jansonius and DC McGregor), pp. 29–50. Dallas: AASP Foundation, 1.

Yamaoka Y, Takimura O, Fuse H and Murakami K (1999) Effect of glutathione on arsenic accumulation by *Dunaliella salina*. *Applied Organometallic Chemistry* **13**, 89–94. https://doi.org/10.1002/(SICI)1099-0739(199902)13:2<89::AID-AOC803>3.0.CO;2-L